BREAKING THE LIMITS OF GAMMA-RAY SPECTROMETRY BY EXPLOITING SPARSITY OF PHOTON ARRIVALS

Samira Carolina Sánchez El Ryfaie[⋆] *and Miguel Heredia Conde*[†‡]

[⋆]Nuclear Physics Laboratory, Simón Bolívar University. Caracas, Venezuela
[†]Center for Sensorsystems, University of Siegen, Paul-Bonatz-Str. 9-11, 57076 Siegen, Germany.
[‡]Dept. of Electrical and Electronic Engineering, Imperial College London, London SW7 2AZ, U.K.
E-mails: samirasancheze@gmail.com • heredia@zess.uni-siegen.de

ABSTRACT

State-of-the-art gamma-ray spectrometry suffers from physical limitations of the sensing system. Pulse pile-up and dead time losses lead to wrong measurements of both the number of pulses and their amplitude. Current techniques based on maxima detection, be in analog domain or after fine digitalization, offer limited resolution, bounded by the instrument response function (IRF). In this work we show how spectral sampling can help breaking the current limits of gamma-ray spectrometry. By means of a sparsity-based sensing model and using a fast and robust parametric spectral estimation method, we show that the unknown parameters, namely time of arrival and energy of the γ-photons, can be accurately estimated from few $m \geq 2K + 1$ frequency samples. In the noiseless case parameter estimation is exact to machine precision and the method has virtually no resolution limit. A thorough experimental evaluation using an empirical IRF unveiled excellent performance, even in overpessimistic conditions.

***Index Terms*—** Gamma-ray spectrometry, sparsity, spectral analysis, superresolution, SPAD

1. INTRODUCTION

Crystal scintillation detectors, coupled to a photomultiplier device such as photomultiplier tubes (PMTs) or silicon photomultipliers (SiPMs), produce a current pulse per each impinging γ-photon, being the pulse amplitude directly related to the energy the γ-photon deposits at the detector. In gamma spectrometry the amplitudes registered for a large set of γ-photon arrivals are used to construct a histogram. Such a histogram or *energy spectrum* can be used to identify the presence of radioisotopes and quantify them. Relevant parameters in nuclear spectroscopy are the energy resolution, pulse *pile-up*, and dead time losses [1].

Within any radiation field there are photons of different energies, but even in the case that photons of the same energy interact with the detector, they will produce pulses with slightly different amplitudes. For radiation of a given energy, this variability influences the width of the corresponding peak in the histogram of amplitudes. Thus the accuracy of the amplitude estimation determines the effective resolution of the obtained energy distribution. The time intervals between successive γ-photon arrivals are stochastically distributed according to a Poisson distribution. This does not exclude the case of two photons arriving to the detector infinitesimally close to one another, such that they produce a single pulse of larger amplitude. Alternatively, if the time between consecutive arrivals is not so short, the second arrival may produce a distinguishable pulse, still overlapping the tail of the first one. In both cases, if maxima detection is used to determine the amplitude, wrong amplitudes will be recorded. The first process is called coincidence summing peak (separation below the detector's time resolution), while the second is called pulse *pile-up*.

The *dead time* is the amount of time the spectrometric system needs to register and process the arrival of a γ-photon, during which it is unable to respond to another photon. The dead time is sometimes set by processes in the detector or is limited by the associated electronic measuring system. Due to the fact that some γ-photons will arrive at the detector during these dead time intervals, the measured counting rate will be lower than the real one, leading to amplitude underestimation. These errors are known as *dead time losses*.

Electronic readout systems of γ-radiation detectors are typically made of analog stages to bandpass-filter the signal and remove undesired low- and high-frequency noise. The pulse maximum amplitude is recorded by a peak-sensing ADC, that is, the peak is detected analogically and then digitized. Such systems normally discard the pulses affected by pile-up and may overestimate pulse amplitudes, worsening the energy resolution. Additionally, the required time to process an individual pulse limits the maximum counting rate the system can handle without incurring in dead time losses.

To overcome the aforementioned limitations, recent research has focused on uniformly digitizing the detector output signal at high rate and reconstructing the pulses from the samples [2, 3, 4]. This approach requires fast ADCs and the amount of generated data is enormous [4]. Instead of resorting to classical Shannon-Nyquist sampling at exorbitant sampling rates to sense a spiky signal, we propose **sampling in frequency domain** instead (Fig. 1c). This decision follows from basic uncertainty principles that are transversal in science (localization in time domain implies wide spread in frequency and vice versa) and is in line with the novel sampling paradigm of *compressed sensing* (CS) [5, 6, 7]. This scheme captures all signal information with a **minimal amount of measurements**, orders of magnitude fewer than those suggested by the Nyquist rate. Instead of applying classical CS as in [8, 9], we leverage the *finite rate of innovation* of the signal [10] and draw from prior works on parametric time-resolved and multiple-path time-of-flight (ToF) imaging [11, 12, 13, 14]. In short, Fourier samples of a train of Dirac delta functions can be modeled as a sum of cisoids. From the lowest-frequency Fourier measurements the model parameters (amplitude and location of the Dirac deltas) can be accurately estimated with **no intrinsic resolution limit** using fast and robust parametric spectral estimation methods.

2. γ-RAY SPECTROMETRY

Often, in order to detect and identify gamma-emitting radioisotopes contained in a radioactive sample, γ-spectrometric techniques are implemented. For this purpose a variety of detectors exists. Inorganic scintillator detectors offer a good trade-off between efficiency, resolution, and robustness [1]. Detectors of this kind are coupled

to photomultiplier devices (commonly PMTs and, more recently, SiPMs), which transform the scintillation light photons into signal pulses, each of them corresponding to a γ-photon interaction within the detector. The number of pulses registered per second and their amplitudes provide information about the sample radioactivity and which radioisotopes are present in it [1]. Generally, the number of visible and UV photons N emitted by an inorganic scintillator like NaI(Tl) [15] after arrival of an ionizing particle at $t = t_o$ reads:

$$N(t, t_o) = N_o \frac{\tau_\mathrm{d}}{\tau_\mathrm{r} - \tau_\mathrm{d}} \left(e^{-\frac{(t-t_o)}{\tau_\mathrm{r}}} - e^{-\frac{(t-t_o)}{\tau_\mathrm{d}}} \right), \quad t \geq t_o, \quad (1)$$

where N_o is the average number of emitted scintillation photons per unit of gamma quanta depositing energy in the detector, τ_r and τ_d are the rise and decay time constants, respectively [16]. The NaI(Tl)'s τ_d is 250 ns [15]. Although the NaI(Tl)'s τ_r has not been reported by the manufactures, normally it is extremely short compared with τ_d [16] and thus (1) is well approximated by:

$$N(t, t_o) = N_o e^{-\frac{(t-t_o)}{\tau_\mathrm{d}}} \quad (2)$$

The SiPM is a solid state photo-detector made of hundreds or thousands single-photon avalanche diodes (SPADs, operating in Geiger-Mode) in series with quenching resistors (R_q) which stop the SPADs' avalanche. The array SPAD-R_q is called microcell. Scintillation photons (visible and UV) produced by the NaI(Tl) are individually detected by each SPAD of the SiPM and the whole system response is a current pulse whose amplitude is proportional to the total amount of visible and UV photons that impinged the SiPM. The SiPM response to a photon arrival is given by:

$$I(t, t_o) = \begin{cases} I_o \left(1 - e^{-\frac{(t-t_o)}{R_\mathrm{d} C_\mathrm{d}}} \right) & t - t_o \leq t_\mathrm{max} \\ I_\mathrm{max} e^{-\frac{(t-t_o)}{R_\mathrm{q} C_\mathrm{d}}} & t - t_o > t_\mathrm{max} \end{cases} \quad (3)$$

$$I_\mathrm{max} = I_o e^{\frac{t_\mathrm{max}}{R_\mathrm{q} C_\mathrm{d}}} \left(1 - e^{-\frac{t_\mathrm{max}}{R_\mathrm{d} C_\mathrm{d}}} \right), \quad t \geq t_o$$

where C_d and R_d are the superposition of the junction capacitance and resistance of the SPADs, respectively, and t_max is the time at which $I(t)$ reaches its maximum and the quenching starts. Since $R_\mathrm{q} \gg R_\mathrm{d}$, the decay of $I(t)$ is much slower than its rise.

One can define the aggregated zero-centered *instrument response function* (IRF) $\phi(t)$ as the convolution between the signals in (1) and (3) for $t_o = 0$, $\phi(t) = (N(\cdot, 0) * I(\cdot, 0))(t)$. Let the Fourier transform of a time-domain signal $p(t)$ be defined as $\hat{p}(\omega) := \langle p(t), e^{\jmath\omega t} \rangle$ and let $\jmath$ denote the complex unit. Then the Fourier spectrum of the IRF is obtained as:

$$\begin{aligned} \hat{\phi}(\omega) &= \hat{N}(\omega)\hat{I}(\omega)\Big|_{t_o=0}, \quad \text{with :} \\ \hat{N}(\omega) &= N_o \frac{\tau_\mathrm{d}}{\jmath\omega(\tau_\mathrm{r} + \tau_\mathrm{d}) + 1 - \omega^2 \tau_\mathrm{r} \tau_\mathrm{d}} e^{-\jmath\omega t_o} \\ \hat{I}(\omega) &= I_o \Bigg[\frac{\left(e^{-\jmath\omega t_o} - e^{-\jmath\omega t_\mathrm{max}} \right)}{\jmath\omega} \\ &\quad + \underbrace{\frac{1}{\frac{1}{R_\mathrm{d} C_\mathrm{d}} + \jmath\omega} \left(e^{-\frac{(t_\mathrm{max} - t_o)}{R_\mathrm{d} C_\mathrm{d}} - \jmath\omega t_\mathrm{max}} - e^{-\jmath\omega t_o} \right)}_{\text{Avalanche (rise)}} \\ &\quad + \underbrace{\frac{e^{\frac{t_o}{R_\mathrm{q} C_\mathrm{d}} - \jmath\omega t_\mathrm{max}}}{\frac{1}{R_\mathrm{q} C_\mathrm{d}} + \jmath\omega} \left(1 - e^{-\frac{t_\mathrm{max}}{R_\mathrm{d} C_\mathrm{d}}} \right)}_{\text{Quenching (decay)}} \Bigg] \end{aligned} \quad (4)$$

Typically the SiPM is series-connected to a resistor of small value (R_s) and the voltage drop over R_s is read out. The resulting recovery time of the SiPM is then

$$\tau_\mathrm{RC} = N C_\mathrm{d} \left(\frac{R_\mathrm{q}}{N} + R_\mathrm{s} \right), \quad (5)$$

where N is the number of microcells in the SiPM. However, it is possible to avoid the need for R_s by using a transimpedance amplifier (TIA in Fig.1c) as readout circuit, so that $R_\mathrm{s} \approx 0$ and $\tau_\mathrm{RC} = R_\mathrm{q} C_\mathrm{d}$. Fig. 1a shows the IRF $\phi(t)$ of our detector, obtained using a transimpedance amplifier at the SiPM output. The shape of ϕ is mostly determined by the decay time constants τ_d and τ_RC [17].

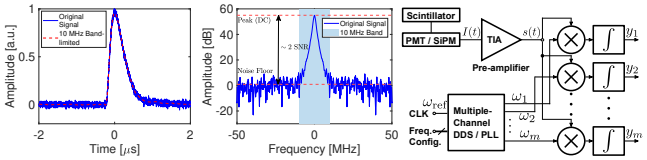

(a) Detector Pulse (b) Spectrum (50 MHz) (c) Schematic

Fig. 1: Voltage pulse generated by our NaI(Tl)-based [15] detector due to the arrival of a γ photon (a). The NaI(Tl) scintilator is coupled to a silicon photomultiplier (SiPM) [18]. The pulse is a bandlimited function, as can be observed in its Fourier spectrum (b). The signal power is concentrated in a narrow bandwidth of approximately 10 MHz (blue shaded areas). The 10 MHz-bandlimited approximation of the pulse is shown with a dashed line in (a). Frequency measurements of the detector output are to be carried out within this bandwidth. A schematic representation of the proposed sensing scheme is provided in (c).

3. SPECTRAL SENSING OF SPARSE PHOTON ARRIVALS

In this section we present the methodology we use to accurately detect and characterize arrivals of γ-photons from few measurements, together with the basic principles we build upon. Let first model the arrival of γ-photons to the detector. Supposing that the detector is placed in the close neighborhood of some radioactive material emitting γ radiation and that we restrict our observations to a period of interest T that is much lower than radioactive decay parameters of the source such as half-life $t_{1/2}$ or mean lifetime τ [19], then the rate at which γ-photons are received at the detector r can be considered to be constant. For T large enough, the expected number of arrivals is $\mathrm{E}[N_\gamma] = rT$. The arrival of the k^th photon is fully characterized by the photon energy Γ_k and time stamp t_k, $\forall k$. Thus the profile of γ-photon arrivals can be modeled as a weighted sum of shifted Dirac delta functions:

$$h(t) = \sum_{k=0}^{K-1} \Gamma_k \delta(t - t_k), \quad 0 \leq t_k < T, \quad (6)$$

where one expects $K \approx rT$ arrivals. The detector itself is composed by a scintillation crystal coupled to an SiPM. The scintillator response to the arrival of a γ-photon at instant t_o is the emission of a number of scintillation photons (visible and UV) given by (1) and the response of the SiPM to each scintillation photon is given in (3). The IRF ϕ is the composition of both responses and its Fourier spectrum is given by (4). We define the set of bandlimited functions $\mathcal{B}_\Omega := \{p : \hat{p}(\omega) = 0,\ |\omega| \notin \Omega\}$. From now on Ω denotes both a frequency region in the continuous case and a set of frequency indices in the discrete scenario. Mostly due to the $\jmath\omega$ terms in the denominators of all addends of $\hat{I}(\omega)$ in (4), most of the signal power of ϕ will be concentrated in a narrow Fourier bandwidth Ω and in practice ϕ is considered to be bandlimited $\phi \in \mathcal{B}_\Omega$.

The IRF ϕ constitutes the actual *probing function* we use to sense $h(t)$ and is given by the hardware. For a given profile of arrivals $h(t)$, the electrical signal at the output of the SiPM is

$$s\,(t) = (h * \phi)\,(t) = \int_{-\infty}^{\infty} h(\tau)\phi(t-\tau)d\tau \tag{7}$$

Provided that (7) can be casted as an elementwise product in Fourier domain, we have that $\hat{s}(\omega) = \hat{h}(\omega)\hat{\phi}(\omega)$, $\forall\omega$, and thus $s \in \mathcal{B}_\Omega$. Furthermore, for any frequency $\omega \in \Omega$, the corresponding Fourier measurement follows the model

$$\hat{s}(\omega) = \hat{\phi}(\omega)\langle h, e^{\jmath\omega t}\rangle = \hat{\phi}(\omega)\sum_{k=0}^{K-1}\Gamma_k e^{\jmath\omega t_k} \tag{8}$$

In this work we propose acquiring a set of (few) m uniform frequency measurements $\vec{y} = \{y_i\}_{i=1}^m$, which follow a measurement model of the shape $y_i = \hat{s}(\omega_i) + n_i$, where n_i is a realization of the i^{th} component of the m-multivariate white Gaussian *measurement* noise. Depending on the spectral sensing hardware the corresponding covariance matrix $\Sigma \in \mathbb{R}^{m\times m}$ may show non-zero off-diagonal components (e. g., due to crosstalk), but here without loss of generality we suppose that $\Sigma := E\,[\vec{n}\vec{n}^*] = \sigma^2\boldsymbol{I}$. From each measurement y_i an estimate of $\hat{h}(\omega)$ can be readily obtained as $\tilde{\hat{h}}(\omega_i) = y_i/\hat{\phi}(\omega_i)$, for $\omega_i \in \Omega$. Due to the pulse shape of ϕ the measurements with largest amplitude will be those of lowest frequency, since approximately $\Delta\log\left|\hat{\phi}(\omega)\right| \propto -\Delta\omega$ (see the triangular shape of the central region of $\hat{\phi}$ in Fig.1b). Thus, for a given measurement budget m, with $\left\lceil\frac{m-1}{2}\right\rceil \in \Omega$, the set of measurements $\vec{y} \in \mathbb{C}^m$ that yields the estimates $\tilde{\hat{h}}(\omega_i)$ with highest signal-to-noise ratio (SNR) is composed of those centered around $\omega = 0$. Provided that we only consider uniform frequency sampling, our measurement model is:

$$\begin{gathered}\tilde{\hat{h}}(\omega_i) = \frac{y_i}{\hat{\phi}(\omega_i)}, \quad y_i = \hat{\phi}(\omega_i)\sum_{k=0}^{K-1}\Gamma_k e^{\jmath\omega_i t_k} + n_i \quad \text{with}: \\ \omega_i = i\omega_0,\ \omega_0 = \frac{2\pi}{T},\ i \in \left\{-\left\lceil\frac{m-1}{2}\right\rceil, \ldots, 0, \ldots, \left\lfloor\frac{m-1}{2}\right\rfloor\right\}\end{gathered} \tag{9}$$

It can be easily shown that $m \geq 2K+1$ measurements are required to estimate the parameters $\{\Gamma_k,\ t_k\}_{k=1}^K$ in (6). We define the oversampling factor $\nu \in \mathbb{N}$ such that the number of measurements is $m = 2\nu K + 1$. For simplicity let $\vec{\mathcal{H}} = \left\{\tilde{\hat{h}}(\omega_i)\right\}_{i=1}^m$ as defined in (9). Retrieving $\{\Gamma_k,\ t_k\}_{k=1}^K$ from $\vec{\mathcal{H}}$ is the classical line spectrum estimation, also known as *Prony's problem* [20, 21] and can be solved using Prony's method (polynomial anihilation) or any of its robust variants [22, 23]. From the latter we adopt the matrix pencil method [23], which provides a fast and robust closed-form (non-iterative) estimate of $\{\Gamma_k,\ t_k\}_{k=1}^K$. We refer to [13] for the derivation of the corresponding Cramér-Rao Lower Bounds (CRB).

The pipeline outlined in this section has been successfully demonstrated in a variety of works related to time-resolved imaging [11, 14], in which ToF pixels are used to gather the measurements. In [14] an intrinsic harmonic cancellation is implemented, so that the ToF pixels directly obtain Fourier measurements of the environment response function. Similarly, we foresee a hardware implementation to obtain all measurements $\vec{y}$ in a single sensor readout, using a set of $m \propto K$ single-frequency filters, i. e., *lock-in* amplifiers (Fig. 1c).

4. EXPERIMENTAL EVALUATION

In this section we use the real IRF of our detector ($\phi(t)$, Fig. 1a) to carry out a highly-realistic evaluation of the methodology outlined in section 3. Our detector is composed by an NaI(Tl) scintillator [15] (420 nm peak) coupled to a SiPM [18] and the output measured via a transimpedance amplifier had $\text{SNR} = 25\,\text{dB}$. The lab radioactive source 137-Cs used for our real experiments has a radioactivity of $0.25\,\mu$Ci, which translates into 9.25×10^3 *counts per second* (cps) average, from which only about 25% interact with the detector [24]. The γ-ray spectroscopic system developed in [25] can register up to 10^4 cps. In sections 4.1 and 4.2 we will consider a worst-case scenario, with a γ-photon arrival rate at the detector of $r = 10^5$ cps, i. e., one order of magnitude larger than the maximum rate in [25].

4.1. Performance in Harsh Realistic Conditions

In this section we evaluate the performance of the proposed approach in harsh realistic conditions, that is, at a high γ-photon arrival rate $r = 10^5$ cps, with overlapping pulses, and in the presence of noise. Given the aforementioned arrival rate, we consider a period $T = 100\,\mu$s, in which $K = 10$ γ-photons arrive to the detector. The results of this simulation are given in Fig. 2 and Table 1. The parameters $\{\Gamma_k,\ t_k\}_{k=1}^K$ were randomly generated from uniform distributions. The proposed method is able to retrieve the signal parameters $\{\Gamma_k,\ t_k\}_{k=1}^K$ (stems) exactly in all low-overlapping cases. For the highly-overlapping case ($\Delta t = 395\,\text{ns}$) reconstruction fails as the SNR decreases. In the noiseless case (omitted) reconstruction is exact to machine precision even for $\nu = 1$.

Table 1: MSE of the vectors of reconstructed time locations and amplitudes, and of the reconstructed signals in Fig. 2 ($K = 10$).

SNR [dB]	$\text{MSE}\left(\{\tilde{t}_k\}_{k=1}^K\right)$	$\text{MSE}\left(\left\{\tilde{\Gamma}_k\right\}_{k=1}^K\right)$	$\text{MSE}\,(\hat{s})$
20	116.33	24.54	1.45×10^{-2}
40	4.46×10^{-6}	1.58×10^{-3}	1.06×10^{-4}
60	2.23×10^{-5}	1.33×10^{-3}	3.92×10^{-5}

4.2. Robustness to Noise

Fig. 2 shows that the estimation error increases with the noise level. Oversampling can counteract the effect of noise. Here we evaluate the effect of noise on the estimation error of $\{\Gamma_k,\ t_k\}_{k=1}^K$ and of the reconstructed signal s for different oversampling factors. The statistics obtained over 100 noise realizations are summarized in Fig. 3. The linearly-decreasing behavior of all curves for sufficiently high SNR illustrates that the CRB is met. SNRs $< 25\,\text{dB}$ are too pessimistic. The operation point of our hardware is marked with a vertical line. Reliable operation at an SNR as low as 20 dB is still feasible using slightly larger oversampling factors, e. g., $\nu = 5$.

4.3. Time Resolution Limit

In this section we address a question of critical importance in practice, namely, how close to each other in time domain can two consecutive γ-photons reaching the detector be and still their corresponding parameters be correctly estimated. The achievable time resolution determines up to which extent pulse *pile-up* can be eliminated. To this end, we evaluate the same reconstruction errors for different Δt ranging from 1 μs to 0. Statistical results over 100 noise realizations are given in Fig. 4. The equidistant parallel lines obtained for different (equidistant) SNRs in all plots for $\Delta t \gtrsim 600\,\text{ns}$ witness agreement with the CRB. As $\text{SNR}\to\infty$, all MSEs $\to\infty$, $\forall\Delta t \in \mathbb{R}\setminus\{0\}$ Our system ($\text{SNR} = 25\,\text{dB}$) could separate photon arrivals 100 ns apart with a time MSE of $-35\,\text{dB}$.

5. CONCLUSIONS

This work deals with the problem of detecting and characterizing the arrival of γ-photons to an inorganic scintillation detector. Each arrival is characterized by a time stamp and an amplitude, related

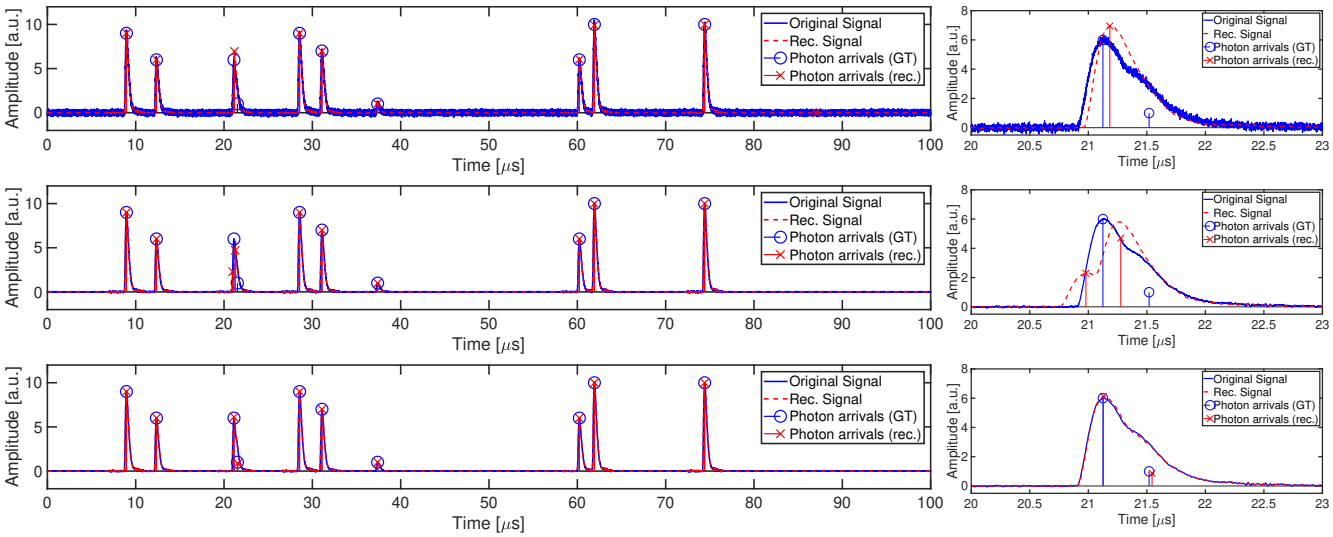

Fig. 2: Original and reconstructed signals from few Fourier samples. Given a randomly-generated set of parameters $\{\Gamma_k,\ t_k\}_{k=1}^{K}$, modeling the energy and arrival times of $K = 10$ γ-photons, a realistic detector output (in blue) is generated by convolving the spikes (blue stems) with a low-passed version of the empirical IRF in Fig. 1a, ϕ. Zero-mean white Gaussian noise is added to the signal to achieve SNRs of 20, 40, and 60 dB (from top to bottom). The locations and amplitudes recovered by the proposed method are represented with red stems. The reconstructed signal (red dashed line) is obtained by convolution with ϕ. A minimal oversampling $\nu = 2$ was used to force a failure case (right plots).

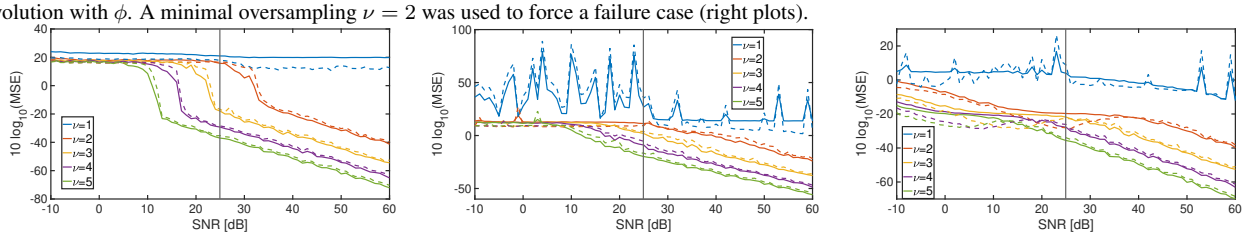

(a) MSE $\left(\{\tilde{t}_k\}_{k=1}^{K}\right)$ vs. SNR (b) MSE $\left(\left\{\tilde{\Gamma}_k\right\}_{k=1}^{K}\right)$ vs. SNR (c) MSE $(\hat{s})$ vs. SNR

Fig. 3: MSE of reconstructed time locations (a), amplitudes (b), and signal (c) versus SNR for different oversampling factors $\nu \in [1, 5]$. The original set of parameters $\{\Gamma_k,\ t_k\}_{k=1}^{K}$ and IRF ϕ was the same used in Fig. 2 ($K = 10$). Solid and dashed lines are mean and standard deviation values computed over 100 noise realizations, respectively. The vertical line points the empirical SNR of our system.

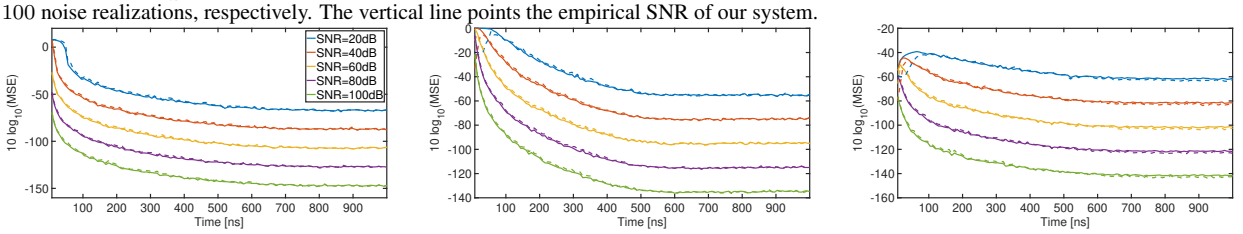

(a) MSE $\left(\{\tilde{t}_k\}_{k=1}^{K}\right)$ vs. Δt (b) MSE $\left(\left\{\tilde{\Gamma}_k\right\}_{k=1}^{K}\right)$ vs. Δt (c) MSE $(\hat{s})$ vs. Δt

Fig. 4: MSE of reconstructed time locations (a), amplitudes (b), and signal (c) versus separation between arrivals Δt of $K = 2$ consecutive γ-photons for different SNRs (SNR $\in [20, 100]$). Fixed oversampling factor $\nu = 5$. Solid and dashed lines are mean and standard deviation values computed over 100 noise realizations, respectively. Single legend in (a).

to the photon's energy. Current approaches based either in analog maxima detection or dense uniform sampling in time domain exhibit limited time resolution and are largely affected by pulse pile-up. We have proposed a shift of the sensing paradigm towards spectral sensing and outlined a methodology that allows reliable estimation of the unknown parameters from a minimal number of samples. In the noiseless case and assuming a perfect pulse model, the method is exact to machine precision, regardless of the time separation between two consecutive photons, that is, it has **no intrinsic resolution limit**.

Immediate future work will focus on a practical hardware implementation of the proposed sensing scheme, prospectively based on a set of analog lock-in amplifiers at the desired frequencies. Further extensions to be explored include one-bit ultra-fast sampling and non-uniform Fourier sampling, the latter of which has been demonstrated for solving a fundamentally equivalent problem in the context of multiple-path ToF imaging in [26].

6. ACKNOWLEDGEMENTS

SCSER thanks Mladen Bogovac for their valuable advise during her stay at NSIL in 2019, as well as LFN-USB and its team for their advise, guidance and support during the development of this work.

7. REFERENCES

[1] G.Knoll, *Radiation Detection and Measurement*, John Wiley & Sons, Inc, Michigan, U.S., 2010.

[2] A. Arriojas, H. Barros, J. Walter, and L. Sajo-Bojus, "FPGA based digital signal processing for high resolution low energy gamma spectrometry," in *X International Symposium on Radiation Physics*, Tuxtla Gutierrez, Mexico, Apr. 2014.

[3] J. Walter, M. Barreiro, L. Sajo-Bojus, E.D. Greaves, and W. Gonzalez, "New approach in add-on multi-channel analyser for gamma ray spectrometry," *Nuclear Instruments and Methods in Physics Research Section A: Accelerators, Spectrometers, Detectors and Associated Equipment*, Apr. 2005.

[4] CAEN, "Digital pulse processing in nuclear physics," `https://www.caen.it/documents/News/32/WP2081\\\_digitalpulseprocessing\_03.pdf`, 2011, [Online; accessed 12-October-2019].

[5] E. J. Candès, J. Romberg, and T. Tao, "Robust uncertainty principles: exact signal reconstruction from highly incomplete frequency information," *Information Theory, IEEE Transactions on*, vol. 52, no. 2, pp. 489–509, Feb. 2006.

[6] E. J. Candès, "Compressive sampling," in *Proceedings on the International Congress of Mathematicians*, Aug. 2006, pp. 1433–1452.

[7] D. L. Donoho, "Compressed sensing," *IEEE Transactions on Information Theory*, vol. 52, no. 4, pp. 1289–1306, Apr. 2006.

[8] B. J. Gestner, "Compressive sensing for nuclear security," Technical report, Sandia National Laboratories (SNL-CA), Livermore, CA (United States), Dec. 2013, [Online: `https://prod-ng.sandia.gov/techlib-noauth/access-control.cgi/2013/1310506.pdf`; accessed 13-October-2019].

[9] L. Raczyński, P. Kowalski, T. Bednarski, P. Bialas, E. Czerwiński, L. Kaplon, A. Kochanowski, G. Korcyl, J. Kowal, T. Kozik, W. Krzemień, M. Molenda, P. Moskal, Sz. Niedźwiecki, M. Palka, M. Pawlik, Z. Rudy, P. Salabura, N. G. Sharma, M. Silarski, A. Slomski, J. Smyrski, A. Strzelecki, W. Wiślicki, and M. Zieliński, "Application of compressive sensing theory for the reconstruction of signals in plastic scintillators," in *Acta Physica Polonica B Proceedings Supplement*, 2013, vol. 6.

[10] M. Vetterli, P. Marziliano, and T. Blu, "Sampling signals with finite rate of innovation," *IEEE Transactions on Signal Processing*, vol. 50, no. 6, pp. 1417–1428, 2002.

[11] A. Bhandari, A. Kadambi, R. Whyte, C. Barsi, M. Feigin, A. Dorrington, and R. Raskar, "Resolving multipath interference in time-of-flight imaging via modulation frequency diversity and sparse regularization," *Opt. Lett.*, vol. 39, no. 6, pp. 1705–1708, Mar. 2014.

[12] A. Bhandari, M. Feigin, S. Izadi, C. Rhemann, M. Schmidt, and R. Raskar, "Resolving multipath interference in kinect: An inverse problem approach," in *SENSORS, 2014 IEEE*, Nov. 2014, pp. 614–617.

[13] A. Bhandari, A. Kadambi, and R. Raskar, "Sparse linear operator identification without sparse regularization? applications to mixed pixel problem in Time-of-Flight/range imaging," in *2014 IEEE International Conference on Acoustics, Speech and Signal Processing (ICASSP)*, May 2014, pp. 365–369.

[14] M. Heredia Conde, T. Kerstein, B. Buxbaum, and O. Loffeld, "Fast multipath estimation for PMD sensors," in *5th International Workshop on Compressed Sensing Theory and its Applications to Radar, Sonar, and Remote Sensing (CoSeRa 2018)*, Siegen, Germany, Sept. 2018.

[15] Saint-Gobain Ceramics & Plastics, Inc., "NaI(Tl) and polyscin NaI(Tl) sodium iodide scintillation material," `https://www.crystals.saint-gobain.com/sites/imdf.crystals.com/files/documents/sodium-iodide-material-data-sheet.pdf`, 2016, [Online; accessed 13-October-2019].

[16] D. McGregor, "Materials for gamma-ray spectrometers: Inorganic scintillators," *Annual Review of Materials Research*, vol. 48, pp. 245–277, Apr. 2018.

[17] SensL, "SiPM biasing and readout," `https://sensl.com/downloads/ds/TN-Biasing\_and\_Readout.pdf`, 2018, [Online; accessed 13-October-2019].

[18] ON Semiconductors, "Arrayj series - silicon photomultiplier (SiPM) high fill-factor arrays," `https://www.onsemi.com/pub/Collateral/ARRAYJ-SERIES-D.pdf`, Jan. 2019, [Online; accessed 13-October-2019].

[19] S. Krane, *Introductory nuclear physics*, John Wiley & Sons, Inc, Michigan, U.S., 1988.

[20] G. Plonka and M. Wischerhoff, "How many fourier samples are needed for real function reconstruction?," *Journal of Applied Mathematics and Computing*, vol. 42, no. 1, pp. 117–137, July 2013.

[21] P. Stoica and R.L. Moses, *Introduction to Spectral Analysis*, Prentice Hall, 1997.

[22] J. A. Cadzow, "Signal enhancement-a composite property mapping algorithm," *IEEE Transactions on Acoustics, Speech, and Signal Processing*, vol. 36, no. 1, pp. 49–62, Jan. 1988.

[23] Y. Hua and T. K. Sarkar, "Matrix pencil method for estimating parameters of exponentially damped/undamped sinusoids in noise," *IEEE Transactions on Acoustics, Speech, and Signal Processing*, vol. 38, no. 5, pp. 814–824, May 1990.

[24] Saint-Gobain Ceramics & Plastics, Inc., "Efficiency calculations for selected scintillators," `https://www.crystals.saint-gobain.com/sites/imdf.crystals.com/files/documents/efficiency-calculations.pdf`, 2016, [Online; accessed 13-October-2019].

[25] S. C. Sánchez El Ryfaie, "Development of a compact, low-power, and low-weight γ-ray spectroscopy system for mobile radiation monitoring," M.S. thesis, Simón Bolívar University, Oct. 2019, To appear.

[26] M. Heredia Conde, A. Bhandari, and O. Loffeld, "Nonuniform sampling of echoes of light," in *Sampling Theory and Applications 2019 (SampTA 2019)*, Bordeaux, France, July 2019.